Thermal-hydraulic modelling of a flexible substation layout for low-temperature waste heat recovery into district heating

Energy 328 (2025) 136386

Contents lists available at ScienceDirect

Energy

journal homepage: www.elsevier.com/locate/energy

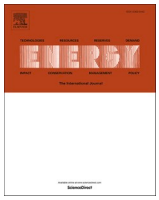

Thermal-hydraulic modelling of a flexible substation layout for low-temperature waste heat recovery into district heating

D. Anania [a,b,*], G. Russo [c], A. Palombo [c], F. Orizio [d], R. Fedrizzi [a], M. Cozzini [a]

[a] Institute for Renewable Energy, EURAC Research, Viale Druso, 1, 39100, Bolzano, Italy
[b] Energy Department, Politecnico di Torino, Corso Duca Degli Abruzzi 24, 10129, Torino, Italy
[c] Department of Industrial Engineering, University of Naples Federico II, P.le Tecchio, 80, 80125, Napoli, Italy
[d] Cogeme Energia, Via XXV Aprile, 18, 25038, Rovato, Italy

ARTICLE INFO

Handling Editor: Neven Duic

Keywords:
Waste heat
District heating
Heat pumps
Energy efficiency
Thermal prosumer

ABSTRACT

This study investigates a thermal substation designed for low-temperature waste heat recovery in district heating networks, where the served user has both heating and cooling demands. The proposed bidirectional substation, equipped with heat pumps and thermal storage units, enables the recovery of excess waste heat in the district heating network and compensates local heating needs when waste heat availability is insufficient. A flexible and detailed TRNSYS-based model is developed to simulate various hydraulic configurations of the substation, tailored for both low- and high-temperature district heating networks, ensuring adaptability to different temperature requirements in diverse applications. The model is applied to a demonstration site in Ospitaletto, Italy, where waste heat is recovered from a steel mill and used to replace gas boilers for space heating and hot water in the factory's canteen and showers. The model's accuracy is validated through a comparison with monitored data, ensuring reliable performance predictions. Performance estimation error is under 5%, demonstrating the model's high reliability. The simulation results show that the system can achieve up to 75% reduction in non-renewable primary energy consumption and carbon emissions, while also allowing the recovery of about 90% of unused waste heat for supply to other connected users.

1. Introduction

The European Union (EU) aims to be climate-neutral by 2050, achieving an economy with net-zero greenhouse gas emissions. This requires a crucial transition towards sustainable production and consumption models [1]. While significant progress has been made in decarbonizing the electricity sector, achieving cost-effective decarbonization of heating and cooling systems remains a major challenge [2]. This is also due to the difficulties in planning and designing 'Thermal Energy Communities' [3].

Heating and cooling for residential, industrial, and commercial sectors represent about 50% of the final energy consumption and contribute to almost one-third of the energy-related CO2 emissions in the EU [4]. District Heating and Cooling (DHC) networks have been acknowledged as a promising solution for the reduction of both primary energy consumption and local emissions to meet the heating and cooling demands of buildings. Even today, these systems largely rely on fossil fuels [5]. Significant efforts are still required to achieve efficient district heating systems, according to the definition in the Energy Efficiency Directive. In addition to higher adoption of renewable energy sources, there is also a significant need for increased use of waste heat as a heat source in district heating systems: the focus on recovering waste heat through district heating systems is expected to be a key priority for the coming years.

Different studies report that the amount of industrial waste heat available along with its respective thermal levels has made it one of the most used heat sources to increase the efficiency of thermal networks since the 1980s. Papapetrou et al. [6] estimate the technically available industrial waste heat in the EU, categorized by sector, temperature level, and country. The available waste heat can be recovered and reused within the same entity to improve its energy efficiency. Various technologies and applications for waste heat recovery and reutilization in industrial processes are discussed in [7]. However, large quantities of waste heat are available at *low temperatures*, making recovery more

This article is part of a special issue entitled: SDEWES 2024 published in Energy.

* Corresponding author.
E-mail address: daniele.anania@eurac.edu (D. Anania).

https://doi.org/10.1016/j.energy.2025.136386
Received 20 December 2024; Received in revised form 17 April 2025; Accepted 30 April 2025
Available online 2 May 2025

challenging. Besides the discrepancies in thermal levels, the recovery and local reuse of low-temperature waste heat present additional difficulties, including temporal mismatches with demand and high recovery costs, as highlighted in [8]. The authors also outline current technologies and future prospects in [8]. They highlight the critical role of heat pumps , thermal storage, and thermal networks in bridging the temporal and spatial gaps between heat availability and demand. Lund et al. [9] suggest that district heating networks can be particularly advantageous for integrating low-temperature waste heat, with the feasibility and efficiency of recovery significantly influenced by the temperature of the network. They point out that new generations of district heating systems could further improve this process. By optimizing the control strategy, the recovery of waste heat in low-temperature district heating networks, such as fifth-generation district heating and cooling (5GDHC), can lead to significant energy savings and improved system efficiency [10]. Furthermore, adjusting the setpoint temperatures for space heating and cooling demands in connected buildings can enhance the flexibility potential of district heating and cooling systems [11].

Despite these challenges in integrating low-temperature waste heat into district heating systems, several studies show innovative solutions and their potential benefits. Fang et al. [12] propose methods for collecting and distributing low-temperature industrial waste heat, improving energy efficiency and reducing environmental impact, as demonstrated in a case study from Chifeng, China. In [13], the use of waste heat from data centers in Finland and its impact on the energy efficiency of district heating systems is analyzed. Khosravi et al. [14] explore the recovery of waste heat from data centers and 5G smart poles to support the district heating network in Espoo, Finland. Fitó et al. [15] optimize the design of a low-temperature industrial waste heat recovery system for district heating in France, using energy and exergy indicators. Fang et al. [16] presents an approach for utilizing industrial waste heat in district heating in northern China, showing benefits in energy efficiency and CO_2 emission reductions. Li et al. [17] examine the integration of surplus heat from steel plants to reduce coal consumption in China's district heating systems, demonstrating feasibility and environmental benefits through a large-scale demonstration project. In [18], the potential heat sources for large heat pumps in Danish district heating systems are investigated, focusing on the feasibility of using low-temperature waste or ambient heat. The results emphasize the importance of seawater as a heat source.

This increasing focus on low-temperature waste heat recovery underscores its potential as a key strategy for enhancing district heating systems. In many cases, these sources are associated with a concurrent heat demand, enabling them to function simultaneously as both heat consumers and producers. This dual role, where the system can both extract and supply heat to the network depending on the circumstances, aligns with the concept of a *thermal prosumer*, as introduced by Brange et al. [19]. Several studies have investigated the integration of prosumers into district heating networks from different perspectives. Brand et al. [20] analyzed the implications of integrating prosumers on supply temperature and pressure variations. Huang et al. [21] examined the contribution of decentralized heat production units to the overall heat generation. The work of Postnikov et al. [22] focused on optimizing load distribution and improving system reliability when prosumers are involved. Kauko et al. [23], as well as Nord et al. [24], evaluated the energy performance and environmental impacts of networks that include prosumers. Finally, Li et al. [25] assessed the economic implications of the operating temperatures of heat-prosumer-based networks.

A user with a heating demand could become a producer for a DH system in the presence of local heat sources, such as solar collectors, or when there is a cooling demand that produces waste heat, as in the case of industrial cooling circuits, data centers, and supermarkets. While local heat reuse is always prioritized, in cases of excess heat compared to the user demand, the substation must feed the surplus into the network.

Table 1
Summary of prosumer substation models in the literature, highlighting the presence of key components and the consideration of simultaneity between heat demand and local heat production or waste heat availability.

Reference	HEX	HP	TES	Hydraulics	Load simultaneity
[23]	✓	×	×	×	×
[29,30]	✓	✓	✓	×	✓
[31]	✓	×	✓	×	✓
[32]	✓	×	×	×	✓
[33,34]	✓	✓	×	×	✓
[35]	✓	×	×	×	✓
[36]	✓	×	×	✓	✓

Conversely, any heat shortage is compensated by the network, which acts as a heat source, similar to traditional DH systems [26]. Therefore, a bidirectional connection is required, enabling the substation to both extract and inject heat into the network, according to its needs. When integrating a prosumer into a DH system, the thermal substation and its impact on the thermo-hydraulic parameters of the network play a crucial role [27]. The substation must be able to meet both heating and cooling demands (even simultaneously) while also supplying heat to the network under the temperature and pressure conditions imposed by the DH operator [28]. Depending on the temperature levels of the user's heat demand, the local availability of heat/waste heat, and the thermal network, different hydraulic configurations of the prosumer substation may be required, with or without the necessity of using a heat pump to adjust temperature levels accordingly. The complexity of these systems has led to growing interest in recent years in modelling prosumer substations. Table 1 summarizes the main prosumer substation models found in the literature. For each model, the presence of heat exchangers (HEX), heat pumps (HP), thermal energy storage (TES), and hydraulic components (valves, circulation pumps, and piping) is specified. Additionally, the possibility of simultaneous heat demand and local heat production or waste heat availability is indicated.

The analysis of existing models in the literature reveals that little effort has been devoted to the detailed modeling of the hydraulic components of the substation, despite their crucial role in accounting for heat losses, pumping energy consumption, and enabling more advanced control strategies. When a heat pump is included, it is typically modelled using the Carnot COP without considering the actual dynamic behavior of the machine. Additionally, the hydraulic configuration of the HP-based substation is fixed, meaning that the connection between the heat load/source and the heat pump is predefined, which limits operational flexibility and adaptability to different cases. Finally, the coupling of heat pumps with thermal storage is often managed through simplified control strategies that do not accurately reflect real-world implementations. These limitations highlight the need for more advanced modelling approaches capable of capturing the complexity of prosumer substations, ensuring a more realistic representation of their operation and control within district heating networks.

In this work, a model of bidirectional substation for low-temperature waste heat recovery in district heating networks is proposed. The substation incorporates heat pumps and thermal energy storage and includes a detailed representation of hydraulic components such as valves, circulation pumps, and piping. The heat pump is modelled dynamically, accounting for the actual compressor operating cycle. Multiple temperature sensors are included to monitor the state of the thermal storage and to select the operating scheme based on thermal levels. The model is implemented in a fully general and flexible manner, allowing its application to a wide range of hydraulic configurations and operational scenarios.

The proposed advanced model has been applied to an Italian case study involving low-temperature waste heat recovery from a steel mill. This application has demonstrated the model's flexibility in adapting to

simpler substation configurations while also serving as a validation case study. The case study analysis further demonstrates that the proposed model is a valuable tool for:

- Performing dimensioning and optimization analyses tailored to the requirements of bidirectional substations
- Testing and defining control strategies to ensure efficient and reliable operation, considering the dynamic interactions between the heat pump, thermal storage, and the network
- Estimating seasonal performance and quantifying the impact of prosumer integration into district heating networks

The results of the simulation confirm the system's effectiveness, showing that, compared to a conventional gas boiler, it can achieve up to a 75 % reduction in non-renewable primary energy consumption and carbon emissions while enabling the recovery of about 90 % of unused waste heat for supply to other users connected to the local district heating network.

The work is organized into four sections. The methodology section describes the case study to which the developed model was applied. Additionally, the modelling of individual substation components and control logic is provided. This is followed by the model validation analysis with real-world monitoring data. Then, the results from the investigated scenarios are discussed, and finally, the conclusions are presented.

2. Methodology

This section is structured in two main parts. First, a detailed description of the reference scenario and the implemented waste heat recovery substation is provided. Then, it presents a simulation model, along with the definition of the Key Performance Indicators (KPIs) used to compare the different scenarios.

2.1. Case study description and investigated scenarios

This section reports the description of a real application of low-temperature waste heat recover installed at a steel mill in Ospitaletto, a municipality in the province of Brescia, Italy.

2.1.1. Reference scenario

The layout of the district heating network in Ospitaletto before the installation of the waste heat recovery substation is represented in Fig. 1.

It fully aligns with the concept of a *neutral-temperature district heating network* with decentralized heat pumps, as discussed in [37], which also provides further details on the Ospitaletto system. The primary heat source is low-temperature waste heat recovered from the cooling circuit of the factory, before being connected to cooling towers. The recovery is performed through a 1.5 MW heat exchanger (source *s1*). The other heat source is groundwater wells (source *s2*). In the current scenario, the heat exchanger for waste heat recovery is sized to fully meet the peak demand of all users connected to the DH network. As a result, groundwater wells are used as a heat source only when waste heat is unavailable.

Groundwater has a temperature of around 15 °C with negligible variability throughout the year, while the temperature of the waste heat depends on the wet bulb temperature of the ambient air and ranges between 20 and 35 °C. The heating demand of the foundry for space heating and domestic hot water production is met entirely by gas boilers. The consumers are mainly schools and multifamily buildings equipped with heat pump substations to raise the temperature level. A centralized pumping station near the groundwater wells ensures water circulation within the network [37,38].

2.1.2. Upgrade scenario

In the upgraded system, illustrated in Fig. 2, a waste heat recovery substation has been installed at the steel mill. The substation is designed to replace gas boilers for space heating and domestic hot water production by utilizing the low-temperature waste heat available from the foundry's cooling circuit. Waste heat is recovered via an additional heat exchanger operating in parallel with the one previously installed. Any surplues waste heat, not required to meet the foundry's internal heating demand, can be fed into the district heating network. Owing to the bidirectional connection, when waste heat is not available, the HP-based substation can draw energy from the neutral-temperature district heating network by extract heat from groundwater wells.

With the installation of the waste heat recovery substation, ASO steel mill has become a heat prosumer within the district heating system. Therefore, the section of the network connecting the foundry to the centralized pumping station was upgraded to operate bidirectionally by adding a bypass branch to the centralized pumps. The scheme of the substation is shown in Fig. 3.

The heat exchanger kit is installed near the cooling towers, close to the connection point with the thermal network. The heat pump room, which houses a heat pump and a storage tank, is located next to the canteen and changing rooms. The distance between the heat exchanger kit and the heat pump room is approximately 130 m; therefore, heat losses and electricity consumption for pumping in this section are not negligible.

The heat exchanger kit includes a 150 kW plate heat exchanger and a bidirectional hydraulic connection with the district heating network, as

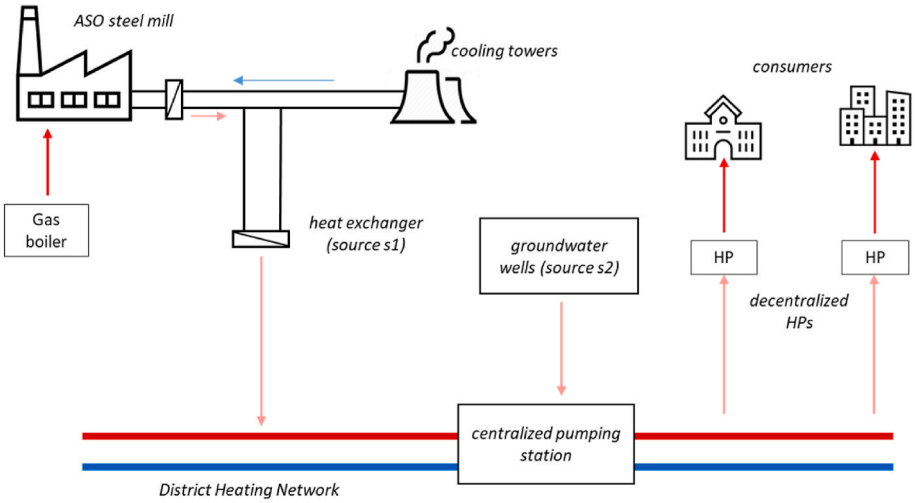

Fig. 1. Layout of Ospitaletto district heating before the waste heat recovery installation.

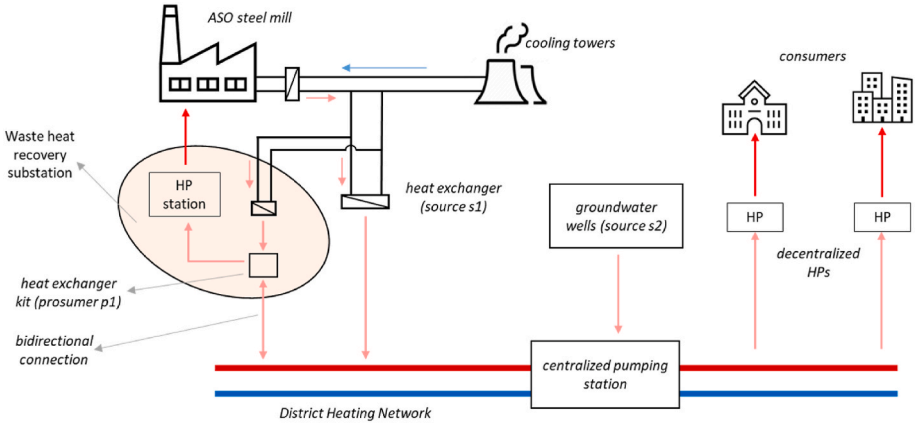

Fig. 2. Current layout of Ospitaletto district heating.

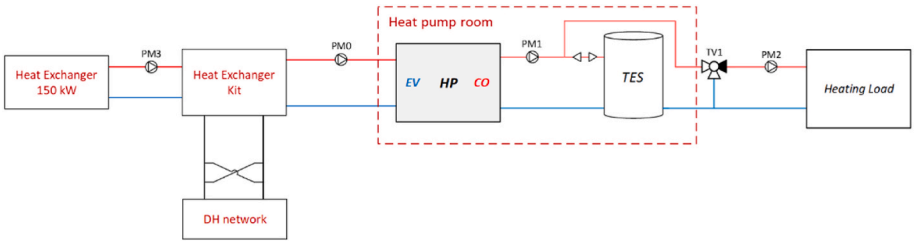

Fig. 3. Low-temperature waste heat recovery substation of ASO steel mill.

shown in Fig. 4. The bidirectional flow is enabled by the two sets of paired three-way valves.

Circulation loop 1.a is activated when extracting heat from the DH network (consumer mode), while *circulation loop 1.b* is activated during heat recovery into the DH network (producer mode). Heat is supplied to the heat pump evaporator via *circulation loop 2*. Finally, *circulation loop 3* enables waste heat recovery from the cooling circuit through the heat exchanger.

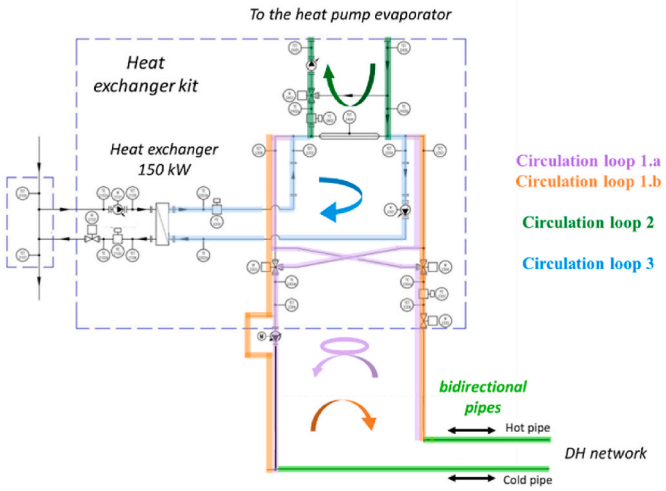

Fig. 4. Schematic representation of the heat exchanger kit installed at ASO steel mill, including the bi-directional hydraulic connection with the district heating network and the three circulation loops for heat extraction, heat recovery, and waste heat utilization (courtesy of Cogeme).

Under the current operating conditions, the network heat demand can be fully met by the existing 1.5 MW heat exchanger. Therefore, the recovery substation is not expected to operate in producer mode, and *circulation loop 1.b* is anticipated to remain inactive. However, the system has been designed with future developments in mind, where an increase in network demand may require the substation to operate as a heat producer. A limit scenario considering this operating mode is discussed in the following section.

The thermal storage tank has a volume of 3,500 L and a setpoint temperature of 55 °C, enabling it to meet both the domestic hot water and space heating requirements of the steel mill. While a supply temperature of 55 °C is required for DHW, the space heating system operates according to a climate curve, with temperatures ranging between 40 °C and 50 °C. By setting the storage setpoint temperature to the highest required level (55 °C), both demands can be satisfied. According to the heat pump datasheet, the nominal heating capacity and the nominal COP are 115 kW and 3.6, respectively. The heat pump is equipped with two fixed-speed scroll compressors operating in parallel. The circulation pumps PM0 and PM1 are modulating and controlled to ensure a 5 °C temperature difference on both the evaporator and condenser sides. Pump PM2 operates to meet the internal heating demand of the foundry, while pump PM3 circulates water on the secondary side of the heat

Table 2
Features of the hydraulic circuits of ASO steel mill.

Circuit	Pump	H'_{rat}	L
Heat pump source-side: connection between heat exchanger kit and heat pump evaporator	PM0	205 kPa	2 × 130 m
Heat pump load-side: connection between heat pump condenser and thermal energy storage	PM1	80 kPa	2 × 5 m
User's distribution: connection between thermal energy storage and user's facilities	PM2	350 kPa	2 × 30 m
Waste heat recovery: connection between recovery heat exchanger and heat exchanger kit	PM3	50 kPa	2 × 15 m

exchanger to recover waste heat. The rated pressure heads and the total lengths of the hydraulic circuits - used to estimate the electrical consumption of the circulation pumps and the thermal losses along the pipes - are summarised in Table 2.

2.1.3. Optimal upgrade scenario

To evaluate potential future developments of the Ospitaletto district heating network, an optimal upgrade scenario is analyzed. This scenario assumes that heat demand on the network has increased to the extent that all excess waste heat available for the substation can be recovered and utilized within the network.

2.2. Modelling

The hydraulic configuration of the substation can vary significantly depending on the thermal requirements of the user and the district heating network operating temperature. When temperature levels are insufficient for direct heat exchange, heat pumps become necessary to satisfy user needs and/or to adjust the temperature levels for the waste heat recovery in the DH network. To minimize the electricity consumption of the heat pumps and to maximize passive heat sharing, an appropriate hydraulic scheme is essential. In scenarios with different temperature generations and demands, an optimal solution could involve hydraulic configurations capable of supporting multiple operating modes, dynamically selecting the most efficient one based on the working temperature conditions [39,40].

In this section, a detailed model of a substation for low-temperature waste heat recovery in district heating systems – developed in TRNSYS 18 – is proposed. The model is designed with a versatile general substation configuration, allowing it to simulate a wide range of real-world applications with varying setups. Its adaptability is ensured by the integrated hydraulic connections, control logics, and the adopted approach, which maintain high accuracy in addressing both thermal and hydraulic factors. In addition to the network temperature profiles and user demand profiles, which are described in the following sections, another boundary condition imposed on the model is the ambient temperature profile. The following sections detail the general model and its specific adaptation to the case study under investigation.

2.2.1. Substation description

The proposed substation is the interface between the district heating network and a building with both a heating demand and a cooling process that generates waste heat. The goal of the substation is to cover the heating demand by utilizing the available waste heat.

As schematised in Fig. 5, the waste heat recovery substation is divided into two sections: the heating and the cooling module.

The heating module is responsible for meeting the building's heating demand, which includes space heating and domestic hot water production. Conversely, the cooling module is designed to serve a generic cooling process while recovering its waste heat. The recovered heat can either be utilized by the heating module or fed into the district heating network, acting as a heat producer. In cases of waste heat shortage, the heating module can also draw heat from the district heating network, functioning as a heat consumer. Therefore, a bidirectional connection between the district heating network and the thermal prosumer substation is required. This is ensured by the hydraulic kit, which enables heat exchange in both directions.

With reference to the detailed representation of the substation shown in Fig. 6, the following sections provide a description of the model of each component.

The figure illustrates the general substation configuration implemented in the model, which includes two *HP + TES blocks* – one in the heating module and one in the cooling module. Each block comprises a heat pump station, a thermal storage unit, and a circulation pump. These components play a crucial role in ensuring efficient operation: heat pumps adjust the temperature levels between the source and the load, while thermal storage tanks enable the decoupling of production from demand, allowing for more flexible module management. The hydraulic kit acts as the interface between the modules and the DHC network, providing a single point of connection.

In many real-world situations, not all components depicted in the general configuration are necessary. The model is designed to simplify the layout by deactivating unnecessary components, making it adaptable to less complex substation configurations. For the case study analysis reported in this work, the model was configured as follows:

- In the heating module, the operating scheme of *Heat Pump Station 1* is fixed and designed to connect the heat source (i.e., the hydraulic kit) to the evaporator and the heating load to the condenser of the heat pump. In this configuration, the heat pump ensures hydraulic separation between the load and the source
- In the cooling module, the *HP + TES block* is deactivated, as it is not present in the real configuration. Therefore, the cooling load exchanges heat directly with the hydraulic kit.

2.2.2. Heat pump stations

The heat pump stations are the core part of the substation since their purpose is to provide the user with the required thermal and/or cooling power at the required temperatures. They are thermo-hydraulic blocks containing one or more heat pumps connected to work in parallel or in

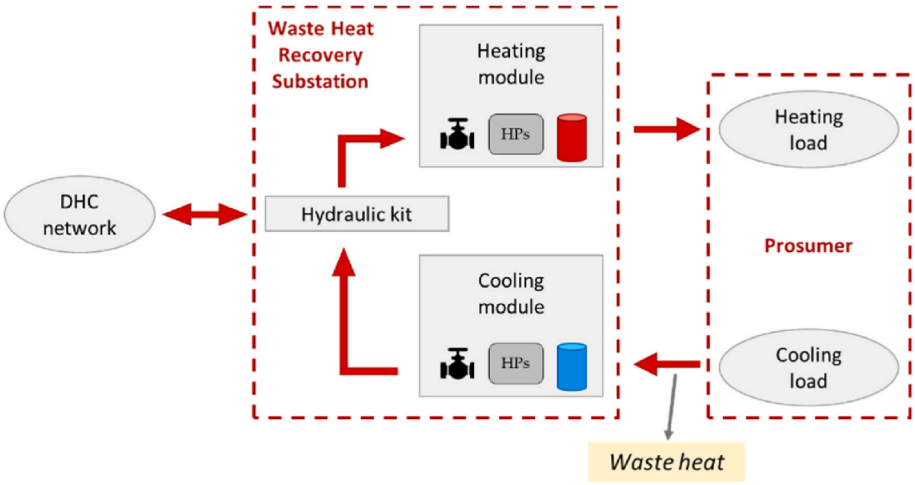

Fig. 5. Waste heat recovery substation schematization.

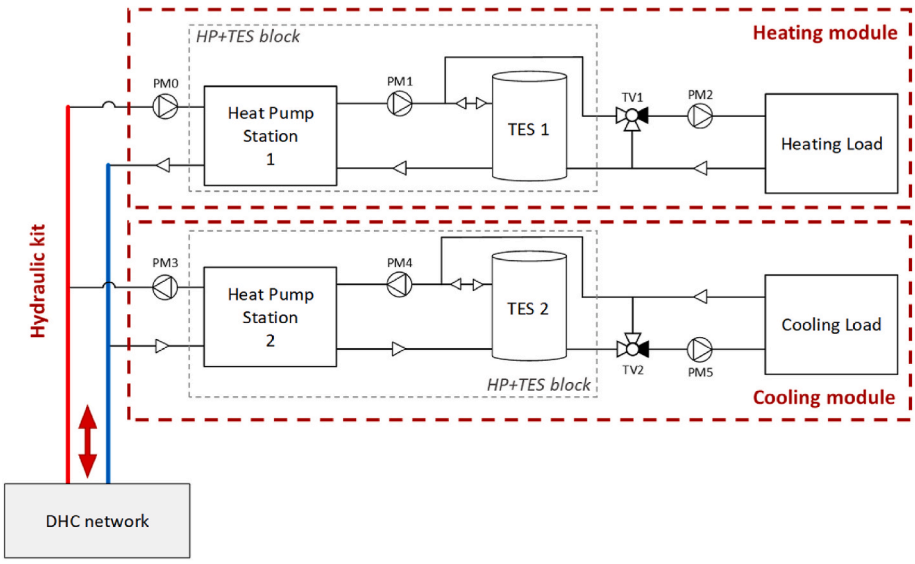

Fig. 6. General configuration of the substation.

series according to requirements. The hydraulic configuration of the heat pump station allows for different operating modes. The selection of the operating mode is based on the inlet temperatures on the source side and the load side, as well as the setpoint temperature to be ensured at the outlet of the load side. The selection of the operating mode is made to ensure higher COP values while also preserving the operating temperature limits of the HP, particularly by considering the maximum allowable inlet temperature at the evaporator. Further details can be found in [40]. Among the various operating modes, there is also the passive heat exchange mode (i.e., heat pump bypass). In this configuration, the thermal levels of the heat source and the heat load are sufficient to allow direct heat transfer without operating the heat pump.

Heat pumps. Heat pumps are modelled using an in-house model developed by the Institute for Renewable Energy of Eurac Research. A single-stage heat pump with a variable-speed compressor is represented in the model. Rather than modelling the individual components and the thermodynamic cycle, the model relies on performance data provided via an external file.

Thermal capacitive effects are not considered in the model, as it is assumed that the heat capacity of the components has a negligible impact on the overall heat exchange of the machine. However, the transient operation of the compressor, including acceleration and deceleration, is taken into account. Consequently, the model requires an appropriate simulation timestep, which should not exceed 10 min. Both modulating and non-modulating compressors are modelled.

The limit temperatures, related to the operative envelope of the compressor, can be set as parameters. If during the simulation the inlet temperature at evaporator or condenser exceeds the operative range, the model immediately switches off the heat pump by resetting the compressor speed.

The model inputs are summarised in Table 3.

The start-up signal for the heat pump is triggered based on the state of the storage tank (the control logic governing the storage is described in the following section). The setpoint temperature defines the target

Table 3
Inputs of the heat pump model.

On/Off signal
Evaporator inlet temperature – $T_{in,ev}$
Condenser inlet temperature – $T_{in,co}$
Evaporator mass flow rate – $\dot{m}_{ev}$
Condenser mass flow rate – $\dot{m}_{co}$
Setpoint temperature – *TSP*

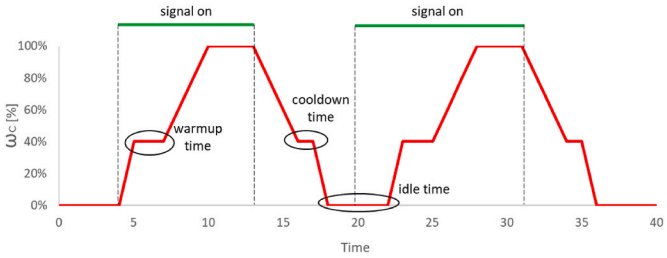

Fig. 7. Example of operating cycle of the HP compressor.

outlet temperature, either at the condenser or the evaporator side, depending on whether the heat pump is operating in heating or cooling mode. The compressor speed, ω_c, is regulated by an internal algorithm that continuously adjusts the operation to follow the desired outlet temperature. This control algorithm considers the warm-up time, cool-down time, and idle time of the machine, which are defined as fixed parameters within the model. Fig. 7 illustrates an example of the compressor operating cycle. The minimum normalised compressor speed is set to 40 % in the example. Once the start-up signal is received, the compressor begins to ramp uo; however, before reaching maximum speed, it remains at the minimum speed for the duration of the warm-up time. When the start-up signal turns off, the compressor starts to ramp down but stays at the minimum speed for the cool-down time before shutting off. Upon receiving a new start-up signal, the compressor re-starts only after the idle time has elapsed.

Regarding the model outputs, based on the input performance data, the model computes the thermal power delivered by the condenser ($P_{th,co}$) and the electrical power consumption of the heat pump ($P_{el,hp}$) using equations (1) and (2).

$$P_{th,co} = a_o + a_1 \cdot T_{in,ev} + a_2 \cdot T_{in,co} + a_3 \cdot \omega_c + a_4 \cdot \dot{m}_{co} + a_5 \cdot \dot{m}_{ev} \quad (1)$$

$$P_{el,hp} = b_o + b_1 \cdot T_{in,ev} + b_2 \cdot T_{in,co} + b_3 \cdot \omega_c + b_4 \cdot \dot{m}_{co} + b_5 \cdot \dot{m}_{ev} \quad (2)$$

In these equations, the coefficients a_0, a_1, a_2, a_3, a_4, a_5, b_0, b_1, b_2, b_3, b_4, and b_5, are calibration parameters obtained through a linear regression of the performance map provided in the heat pump's datasheet. These coefficients account for the influence of the inlet evaporator temperature, the inlet condenser temperature, the evaporator and condenser mass flow rates, and the compressor speed on the heat pump's performance, allowing the evaluation even under off-design conditions.

2.2.3. Thermal energy storages

Thermal energy storages are modelled using TRNSYS Type 340 [41]. The fluid in the storage is modelled as several fully mixed nodes of equal volume. To strike a balance between result accuracy and computational effort, the number of nodes is set to 30.

The storage is a cylindrical tank without an internal heat exchanger, meaning that water flows through and is drawn directly from the tank. To limit heat loss to the ambient, a thickness of thermal insulation can be considered when calculating the overall heat transfer coefficient of the storage tank (UA_{TES}) according to equation (3).

$$UA_{TES} = \frac{1}{\frac{1}{\alpha_{int} \cdot A_{int}} + \frac{\ln(D_{ext}/D_{med})}{2\pi \cdot H_{TES} \cdot \lambda_{ins}} + \frac{\ln(D_{med}/D_{int})}{2\pi \cdot H_{TES} \cdot \lambda_{tank}} + \frac{1}{\alpha_{ext} \cdot A_{ext}}} \tag{3}$$

The formula accounts for the different heat transfer mechanisms, including internal convection between the water and the tank's inner surface, conduction through the metallic tank wall and insulation layer, and external convection with the surrounding air.

Control logic of the storage units. If the *HP + TES block* is present, the heat pump stations are responsible for maintaining the storage tanks at an adequate temperature to meet the users' heating and/or cooling demands. As a result, their activation is triggered by a signal from the storage tank, as further discussed in Appendix A. This signal is generated based on readings from two temperature sensors placed at different heights within the tank. Due to thermal stratification, these sensors detect different temperature levels.

Focusing on the storage tank serving the heating load (TES 1 in Fig. 6) and assuming an initial condition where the tank is fully charged, the top sensor detects a gradual temperature decrease as heat is drawn by the user. Once the upper sensor measures a temperature equal to the setpoint, a signal is sent to the heat pump station to initiate the charging cycle. This cycle continues until the bottom sensor registers a temperature above the setpoint, at which point the charging process is stopped. This control logic is visually represented in Fig. 8.

The same dual-sensor control logic is applied to the TES 2 storage tank, which serves the cooling load. By setting the storage tank setpoints to temperature values compatible with the heating and cooling demands, the system ensures that user requirements are consistently met. At the condenser outlet of the heat pump, temperature setpoints are defined to meet the user's heating demand (for the heating module) and the temperature required by the district heating network operator (for the cooling/waste heat recovery module).

2.2.4. District heating and cooling network and hydraulic kit

Since the model focuses solely on the thermal substation, the district heating network is treated as a boundary condition. The temperature profiles of the hot and cold pipes are provided to the model through an external file. The impact of the substation on altering these temperature profiles is neglected, which is a reasonable assumption when the size of the substation is significantly smaller than the transmission capacity of the connected network section.

As the performance of the heat pumps is highly temperature-dependent, it is essential that the hydraulic kit model accurately captures the mixing effects between the different water flow rates. For this reason, an analytical model based on steady-state mass and energy balance equations is implemented.

Referring to Fig. 9, for both hydraulic manifolds the balance equations are given in equations (4) and (5).

$$\sum \dot{m}_{in} = \sum \dot{m}_{out} \tag{4}$$

$$\sum (\dot{m} \cdot T)_{in} = \sum (\dot{m} \cdot T)_{out} \tag{5}$$

At each timestep of the simulation, the known variables include the flow rates and the inlet/return temperatures of the heating and cooling modules, as well as the temperature of the water drawn from the district heating network. The operating mode is determined by the flow rates: if the heating module's flow rate is lower than that of the cooling module, the system operates in producer mode. Conversely, if the heating module's flow rate is higher, the system is in consumer mode. When the substation operates in consumer mode, it draws water from the hot pipe of the DHN, which is at approximately 15 °C, as the heat source is the groundwater wells. Thermal losses along the network are neglected in this assumption. In producer mode, the substation extracts water from the cold pipe of the DHN, which is considered to have a temperature of 8 °C, based on a temperature difference of 7 °C between the hot and cold pipes. Given the small dimensions of the manifolds, both pressure drops and thermal losses are neglected in the model.

2.2.5. Piping, valves and circulation pumps

The pipes are modelled using TRNSYS Type 31, which allows to consider the thermal losses both when the water is stagnant and when it is circulating in the pipes. All the pipe sections within the substation and the connections to the DHC network and the user facilities are considered. The several diverting and mixing three-way valves and thermostatic valves included in the substation are modelled using their respectively TRNSYS Types. The control signal that defines the actuator position and the setpoint temperature of the thermostatic valves are specified in the control unit.

Water flows within the substation are managed by modulating pumps that receive the signal of the required mass flow from the control unit. As each pump has its own permissible mass flow rate range, the actual circulating flow rate may differ from the required one. Since TRNSYS does not allow for the calculation of pressure drops along the circuits, the electricity consumption of the pumps is estimated using a quadratic load curve for each circuit. The pressure head (H') is based on the rated pressure head of the circuit (H'_{rat}), the circulating mass flow rate ($\dot{m}$), and the rated mass flow rate of the circuit ($\dot{m}_{rat}$), according to equation (6).

$$H' = H'_{rat} \cdot \frac{\dot{m}^2}{\dot{m}_{rat}^2} \tag{6}$$

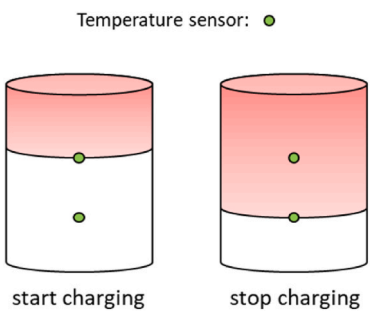

Fig. 8. Two-sensor control logic for the TES.

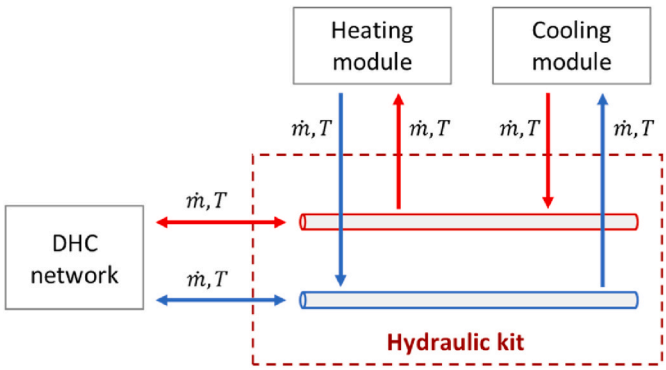

Fig. 9. Input and output variables of the hydraulic kit model.

The rated mass flow rate of a circuit corresponds to its design condition, which is given by the rated thermal power and the design temperature difference between supply and return. Instead, the rated pressure head is given by the sum of the distributed and concentrated pressure drops along the circuit when the rated mass flow rate is circulating. The electrical consumption of the pump is given by equation (7).

$$P_{el,pump} = \dot{m} \cdot \frac{H'}{\rho_{water} \cdot \eta_{pump}} \tag{7}$$

The efficiency of the pump (η_{pump}) is assumed to be constant and equal to 0.6, and the water density (ρ_{water}) is equal to 1′000 kg/m^3.

2.2.6. User loads

The building served by the thermal substation is not included in the model. Therefore, the heating load and the cooling load (waste heat source) along with their respective thermal levels are treated as boundary conditions, provided through external files. The methodology applied to estimate these load profiles is outlined below.

Heating load. The annual demand of domestic hot water (DHW) is estimated according to equation (8) provided by the norm UNI-TS 11300–2:2008.

$$E_{DHW} = \sum (\rho \cdot c)_{water} \cdot V_{water} \cdot (T_s - T_r) \cdot D \tag{8}$$

In the norm, the supply temperature (T_s) and the return temperature (T_r) are assumed equal to 40 °C and 15 °C, respectively. The term *D* represents the number of days for the calculation period, assumed equal to 365. The daily water volume requirement (V_{water}) is calculated as the product of the specific daily demand and an extensive parameter. The value of these two parameters is specified in the standard based on the specific utility. For the canteen, the daily water requirement is 4 L per day per meal, multiplied by 2 meals for every 50 guests. For the changing rooms, it is 100 L per day per shower, multiplied by 20 showers.

The hot water usage profile is provided as an input to the model, and its estimation depends on the type of utility served. The hourly profile used in the analysis is shown in Fig. 10. The higher consumption peaks are referred to the end of the work shift as showers are used, while the lower peaks are referred to the meal periods.

Regarding the space heating (SH) load, the thermal power required to maintain the heated area at the indoor temperature (T_{indoor}) of 20 °C is estimated by considering only the effect of the outdoor temperature, thus neglecting internal and solar gains. Equation (9) is used to estimate the hourly load for space heating.

$$P_{SH,req}(\theta) = P_{SH,nominal} \cdot \frac{T_{indoor} - T_{air}(\theta)}{T_{indoor} - T_{SH,design}} \cdot occupancy \tag{9}$$

The term $P_{SH,nominal}$ refers to the thermal power required for space heating by the building when the outdoor temperature is equal to the design outdoor temperature ($T_{SH,design}$), as defined in standard UNI 5364. The value of $P_{SH,nominal}$ is assumed to correspond to the capacity of the building's heating system. The term *occupancy* refers to the hours during which the building is occupied and, thus, heated. The factory is assumed to be open from Monday morning at 6:00 a.m. to Saturday afternoon at 6:00 p.m. The hourly outdoor temperature profile (T_{air}) for the area under consideration is an input to the model and can be found in [42].

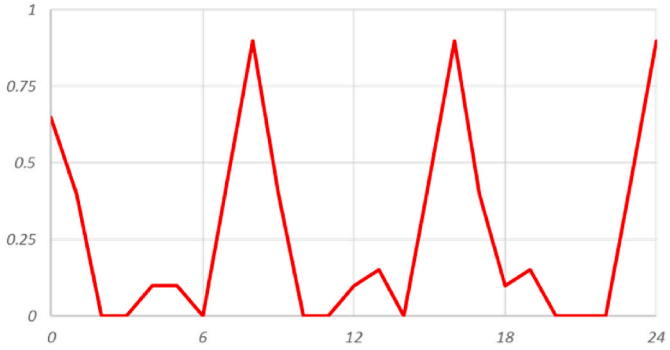

Fig. 10. Daily profile of the domestic hot water load factor.

While the setpoint temperature for DHW remains constant throughout the year at 55 °C, the setpoint for SH follows a climatic curve. Since the model combines these two loads, the setpoint for the thermostatic valve TV1 (see Fig. 6) is computed as the weighted average of the two. This methodology, beside ensuring equivalent mass flow rate tapped from the tank, upholds consistency in the return temperature to the storage tank TES 1, a crucial factor influencing the heat pump performance. The mass flow rate supplied for space heating is calculated based on the required thermal power and the operating temperature difference of the heating terminals, which is a parameter of the model. For the domestic hot water, the external file directly provides the model the required mass flow rate.

Cooling load (waste heat source). The cooling load is represented by a generic cooling process, from which the substation aims to recover extracted heat. The required cooling power (P_{WH}) and the available waste heat temperature (T_{WH}), representing the return temperature from the cooling process, are provided via an external file. Based on these profiles and the temperature difference of the cooling process (ΔT_{WH}), the setpoint temperature of the thermostatic valve TV2 (see Fig. 6) and the circulating mass flow rate are computed according to equations (10) and (11).

$$TSP_{TV2}(\theta) = T_{WH}(\theta) - \Delta T_{WH} \tag{10}$$

$$\dot{m}_{WH}(\theta) = \frac{P_{WH}(\theta)}{c_{p,water} \cdot \Delta T_{WH}} \tag{11}$$

The foundry process is active from Tuesday morning at 8:00 a.m. until Saturday afternoon at 4:00 p.m. The thermal power to be dissipated by the cooling process is much larger than the size of the two recovery exchangers, 1.5 MW and 150 kW. Hence, during the operating period, the recovery heat exchanger of the substation always has the nominal power of 150 kW available. Regarding the available waste heat temperature at the secondary side of the recovery heat exchanger, it was calculated according to the equation (12).

$$T_{WH}(\theta) = max\left(15\ ^\circ C, T_{wb,air}(\theta) + \Delta T_{cooling\ process}\right) \tag{12}$$

The cooling circuit connected to the cooling towers is managed to ensure that the water temperature never drops below 15 °C. The temperature difference of the cooling process accounts for the various temperature drops of the cooling water across the circuit and serves as a calibration factor, which is determined based on the available monitoring data.

2.2.7. Key Performance Indicators

The Key Performance Indicators considered for the analyzed system are the Seasonal COP (SCOP), the Seasonal Performance Factor (SPF), and the non-renewable Primary Energy Factor (PEF_{nren}). The SCOP of the heat pump, defined as $SCOP_{HP} = E_{co,HP}/E_{el,hp}$, represents the ratio between the annual thermal energy delivered at the condenser and the electrical energy consumed by the compressors. The SPF of the substation, calculated as $SPF = E_{th,user}/E_{el,tot}$, expresses the ratio between the net heat supplied to the user and the total electrical energy consumed. Lastly, the PEF_{nren}, expressed as $PEF_{nren} = E_{p,nren}/E_{th,user}$, quantifies the amount of non-renewable primary energy required by the substation per unit of heat supplied to the user.

The non-renewable primary energy consumption associated with electricity use is computed based on the national electricity production

efficiency (η_{grid}), as defined in equation (13). Since the HP-based substation relies exclusively on electricity as its energy input, the PEF_{nren} is derived using equation (14).

$$\eta_{grid} = E_{el,grid} / E_{p,nren,grid} \tag{13}$$

$$PEF_{nren} = E_{p,nren} / E_{th,user} = 1 / (\eta_{grid} \cdot SPF) \tag{14}$$

Term $E_{el,grid}$ represents the electricity consumption drawn from the grid, which, in the analyzed system, corresponds to the total consumption since there are no local electricity generation systems. Using the most recent data available in the report of ISPRA, updated to 2020, [43], and performing the mathematical steps in the equation (15), it is possible to estimate the value of η_{grid}.

$$\eta_{grid} = (E_{el,nren} + E_{el,ren}) / E_{p,nren,grid} = \eta_{th} \cdot (E_{el,nren} + E_{el,ren}) / E_{el,nren}$$
$$\eta_{grid} = 0.566 \cdot (181.3 + 99.2) / 181.3 = 0.875 \tag{15}$$

The term η_{th} denotes the efficiency of the national thermoelectric power generation system. The quantities $E_{el,nren}$ and $E_{el,ren}$ (both expressed in TWh/y) refer to the electricity produced at the national level by thermoelectric power plants and renewable energy sources, respectively. As a result, the parameter η_{grid} differs from η_{th}, since it represents a global efficiency that accounts for the contribution of renewable energy sources to electricity generation. This implies that η_{grid} can theoretically reach arbitrarily high values – approaching infinity – if electricity was entirely generated from renewables.

2.2.8. Comparison with the reference scenario

To assess the impact of replacing gas boilers with the HP-based waste heat recovery substation, the non-renewable primary energy consumption and greenhouse gas emissions of the two scenarios are evaluated according to the equations (16)–(19), and based on the parameters in Table 4.

$$E_{p,nren} = E_{th,user} / \eta_{boiler} + E_{el,PM2} / \eta_{grid} \tag{16}$$

$$M_{CO2,eq} = (E_{th,user} / \eta_{boiler}) \cdot f_{naturalgas} + E_{el,PM2} \cdot f_{electricity} \tag{17}$$

$$E_{p,nren} = E_{th,user} \cdot PEF_{nren} \tag{18}$$

$$M_{CO2,eq} = E_{el,tot} \cdot f_{electricity} \tag{19}$$

Note that equations (16) and (17) refer to the reference scenario, while equations (18) and (19) refer to the upgrade scenario. In the reference scenario, since the heat production relies on natural gas, the corresponding non-renewable primary energy consumption is given by the ratio of the heat supplied to the user and the efficiency of the gas boiler system. The electricity consumption of the circulation pump of the user's distribution circuit, PM2, must also be considered. Instead, for the upgrade scenario, the non-renewable primary energy consumption can be calculated using the corresponding PEF_{nren}.

3. Monitoring data and model validation

The operator of the waste heat recovery substation, Cogeme, provided monitoring data about the real operation of the system. The data collected included:

- Temperature measurements at various points within the substation, recorded every 15 min.
- Heat meters with fixed intervals, which record energy consumption or production after reaching a predefined energy threshold
- Electric energy meters, tracking the electrical consumption of the heat pump and the circulation pumps

Due to the different data frequencies, a preprocessing step was performed to isolate periods of operation where sufficient data were available for comparison with the model's simulations. Although the varying data frequencies prevented a detailed comparison of all system operating dynamics, it was still possible to evaluate the performance during specific operating cycles. This enabled a meaningful validation of the model, with the comparison carried out by calculating the relative error between the simulated results and the monitored data.

The validation process was carried out in a structured manner, assessing both individual components and the overall system performance. In the following sections, detailed analyses are presented for each validation step. First, the temperature profile of the available waste heat was calibrated to ensure accurate representation within the model. Then, the availability of waste heat was validated by comparing the simulated and monitored data. The performance of the HP + TES block was evaluated based on how well the model predicted its operational behavior, followed by a specific validation of the heat pump's model. Finally, the overall performance of the substation was assessed by comparing the predicted and measured performance indicators. The results of each step are discussed in the respective sections, providing insights into the model's accuracy. This block-by-block validation approach ensures that each key component is reliably represented, ultimately confirming the validity of the entire model.

3.1. Waste heat recovery

In Fig. 11 the 15-min monitoring data concerning the waste heat temperature available at the secondary side of the recovery heat exchanger (T_{WH}) are reported. The data refers to an entire week at the end of March 2024.

On Monday, due to the inactivity of the foundry processes, no waste heat was available, and the temperature remained around 15 °C. Starting from Tuesday morning, waste heat became available, and with a temperature profile expected to be influenced by both the pattern of ambient temperature (affecting cooling towers with a day/night effect) and by the intensity of the actual production shifts. Temperature peaks reach up to 30 °C, while the average temperature during the operating period of the foundry process is about 23 °C. Over the weekend, the temperature drops again due to the shutdown of the foundry processes. Based on the available data for T_{WH}, the temperature difference of the cooling process ($\Delta T_{cooling\ process}$) was calibrated to minimize the RMSE over this period, ensuring the best match between the measured profile and the estimate of T_{WH} obtained using equation (12). This equation also includes the wet bulb temperature ($T_{wb,air}$), which is a known profile reported in section 4.1.1.

Considering only the periods when the foundry process was active and the heat pump was operating, and thus when the available waste

Table 4
Gas boiler system efficiency and emission factors.

η_{boiler} [44]	91 %
$f_{natural\ gas}$ [45]	0.235 $t_{CO2,eq}/MWh_p$
$f_{electricity}$ [43]	0.2598 $t_{CO2,eq}/MWh_{el}$

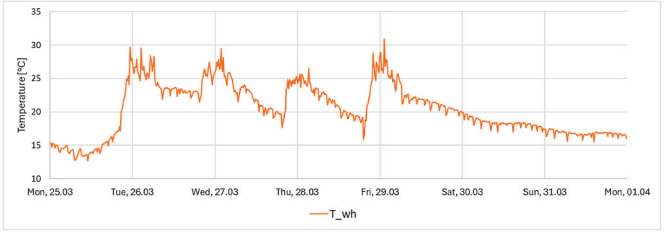

Fig. 11. Monitoring data of the waste heat temperature.

Table 5
Comparison of recovered waste heat and average thermal power over a 20-h period, presenting monitored data, simulated results, and the corresponding relative error.

	Monitored	Simulated	Error
Waste heat recovery	1′411.3 kWh	1′588.9 kWh	+12.6%
Average thermal power	66.8 kW	77.5 kW	+12.6%

heat was recovered and used by the heat pump's evaporator, a comparison was made between the monitored values and those obtained from the simulation. The results for the observed period, which corresponds to approximately 20 h in total, are summarised Table 5.

The relative error is approximately 12.6%, primarily due to the complexity of accurately estimating waste heat availability profiles, which are inherently uncertain. The simulated result relies on a theoretical availability profile, meaning that the discrepancy is not only a consequence of substation model approximations but also of necessary input simplifications. Despite the deviation, the results demonstrate that the simplified approach used to estimate the input profile of the waste heat availability provides a practical balance between accuracy and simplicity. This validation suggests that the methodology remains a rapid and effective option, even without detailed waste heat availability data. A more precise analysis would require detailed availability profiles as direct inputs, but at the cost of increased complexity and data requirements.

3.2. Heat pump and thermal energy storage

The comparison between the monitored and simulated performance values observed on March 28, 2024, is summarised in Table 6.

The heat pump charges the storage tank as soon as it is depleted, following the control logic outlined in the methodology section. Both monitored and simulated data show five operating cycles throughout the day. The errors observed in both the average cycle duration $\Delta\overline{\theta}_{cycle}$ and the average power supplied by the condenser per cycle $\overline{P}_{th,co}$, which are approximately 4% and 7% respectively, indicate that the model is effective in replicating the behavior of the HP + TES block, accurately forecasting the dynamics of the tank's charging and discharging cycles.

The estimate of the resulting heat pump's electricity consumption is accurate, with an error of 1.19%. On the reported day, the heat pump operated using waste heat on the source side, resulting in an average inlet temperature to the evaporator above 15 °C, which corresponds to the temperature of the groundwater wells. The simulation predicted an average $T_{in,ev}$ of approx. 22.6 °C, while the observed data showed a value of 21.0 °C. Since the average inlet temperature to the condenser, $T_{in,co}$, is roughly the same, this results in a slightly higher COP and a higher heat supply at the condenser side estimated by the simulation compared to the actual values.

The detailed comparison of the HP's performance regarding the five operating cycles is provided in Fig. 12.

For each cycle, the estimate of the average return temperature from

Table 6
Comparison between monitored and simulated heat pump performance on March 28, 2024.

	Monitored	Simulated	Error
Number of cycles	5	5	/
$\Delta\overline{\theta}_{cycle}$	43 min	41 min	-3.80%
$\overline{P}_{th,co,cycle}$	145.6 kW	155.1 kW	+7.21%
$E_{th,co}$	520.1 kWh	536.4 kWh	+3.13%
$E_{el,HP}$	118.7 kWh	120.1 kWh	+1.19%
$\overline{T}_{in,ev}$	21.0 °C	22.6 °C	+7.52%
$\overline{T}_{in,co}$	49.0 °C	49.1 °C	+0.20%
COP	4.38	4.47	+1.92%

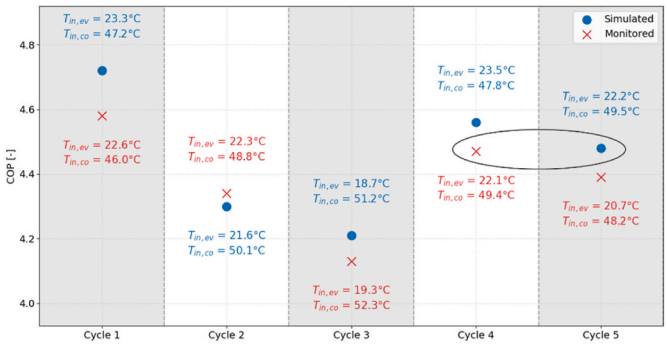

Fig. 12. Comparison of simulated and monitored HP's COP for March 28, 2024. Each cycle is represented along the X-axis, while the Y-axis reports the heat pump's COP. The markers indicate the monitored values (red) and simulated values (blue), with the average inlet temperatures to the evaporator and condenser labelled near the respective points.

the tank to the heat pump is accurate with respect to the monitored values, with a maximum error of −3.2%. This is particularly important because the condenser inlet temperature significantly affects the performance of the heat pump. A larger error is observed in the estimation of the average inlet temperature to the evaporator, with a maximum value of +15.6% observed during the fourth cycle. This error can be attributed to the calibration of the waste heat temperature profile, which inherently introduces some level of approximation. Indeed, calibration involves adjusting the model to match known data, but this process can lead to small discrepancies. Despite this, the analysis demonstrates good agreement between the monitored and simulated values of the average COP, with a maximum relative error of 3% observed during cycle 1. By comparing the performance between the fourth monitored cycle and the fifth simulated cycle (circled in the figure), which are characterised by nearly identical inlet temperatures to both the condenser and the evaporator, a COP of 4.47 is observed for the monitored cycle and 4.48 for the simulated cycle – values that are virtually identical. This reinforces the accurate calibration of the heat pump model, as the calibrated performance map delivers results consistent with those of the actual system under the same input conditions.

3.3. System performance

For the days February 16 and May 3, the readings from the meters installed in the substation are also available. From their difference, the real energy consumption for this period is known. This information allows a comparison between the actual heat supplied to the foundry for space heating and domestic hot water and the estimation using the previously described methodology, which was used as input for the simulation. Additionally, it is possible to evaluate the ability of the model to estimate the system's performance over a longer time period.

As shown in Table 7, an error of approximately 12% was made in estimating the thermal demand during the reported period. This also leads to a higher amount of heat supplied by the heat pump in the simulation compared to the real scenario, as well as an increased consumption of the circulation pump PM1 between the HP and the storage. The estimation of the heat pump's COP is accurate, with an error of about 2%. When considering the heat pump and storage unit as a single system and the corresponding COP, calculated as $E_{th,user}/E_{el,HP}$, a slightly higher but still acceptable error of +4% is observed. The Performance Factor (PF) of the substation is calculated as the ratio between the heat supplied to the user and the total electrical consumption of the heat pump and circulation pumps. The model accurately estimates this value, with an error of approximately 3%.

Based on the observed results, the model can be considered validated, allowing the exploitation of the annual simulation results to estimate the expected performance of the system and its impact on the

Table 7
Comparison of system performance over a two-month period, including integrated energy values and performance indicators, based on monitored data and simulated results.

	Monitored	Simulated	Error
$E_{th,user}$	34.5 MWh	38.5 MWh	+12%
$E_{th,co}$	36.6 MWh	40.1 MWh	+10%
$E_{th,ev}$	28.3 MWh	31.2 MWh	+10%
$E_{el,HP}$	8.34 MWh	8.94 MWh	+7%
$E_{el,PM0}$	0.55 MWh	0.68 MWh	+24%
$E_{el,PM1}$	0.17 MWh	0.19 MWh	+11%
$E_{el,PM2}$	0.09 MWh	0.11 MWh	+18%
$E_{el,PM3}$	0.11 MWh	0.13 MWh	+18%
COP_{HP}	4.39	4.49	+2%
$COP_{HP,TES}$	4.13	4.31	+4%
PF	3.73	3.84	+3%

Ospitaletto district heating network. These analyses are presented in the next section.

4. Scenario analysis and results

The reported analysis aims to estimate the seasonal performance of the waste heat recovery substation, and to estimate the potential impact of the prosumer integration in the network.

Two different network scenarios are investigated in this section. First, a starting and more conservative scenario, referred to as the *upgrade scenario*, is analyzed. This is more representative of the current network situation, where the connected heating loads can already be satisfied with the available sources, and the addition of extra waste heat can barely be exploited. Second, an *optimal upgrade scenario* is analyzed, where the network is assumed to expand its customers (as there are several non-connected buildings along the current pipeline) so that all the available excess waste heat recovered by the ASO HP-based substation could be used, even in summer. To achieve this, the heat demand on the network during the summer must be high enough, which would require connecting new users. The future scenario is likely to fall somewhere between these two extremes, making this analysis a useful reference for understanding the range of possible outcomes.

For the *upgrade scenario*, the results concerning the primary energy and greenhouse gas emission savings achievable by replacing the gas boiler system with the waste heat recovery substation at the ASO steel mill are presented. For the *optimal upgrade scenario*, the amount of waste heat that the system could potentially recover in the district heating network is evaluated, highlighting the benefits of a bidirectional connection.

A timestep of 5 min is used for the simulation.

4.1. Analysis of the upgrade scenario

The hourly profiles of dry and wet bulb temperature in Ospitaletto, shown in Fig. 13, are available for a Typical Meteorological Year (TMY) in [42].

The design outdoor temperature for the space heating system in Ospitaletto is −7 °C, and its capacity is 50 kW. Applying the methodology described, this results in an annual space heating load of approximately 96 MWh. The annual hot water demand for the canteen and changing rooms is estimated at around 26 MWh. Based on the assumed operating profiles for the foundry process and the size of the substation's heat recovery exchanger, the total availability of waste heat is approximately 819 MWh.

The results related to the annual value of the main energy flows for the upgrade scenario are summarised in Table 8.

The substation does not rely on fossil fuels, it has only electricity consumption. In addition to the annual electricity consumption of the heat pump, the consumption of all the local circulating pumps is also

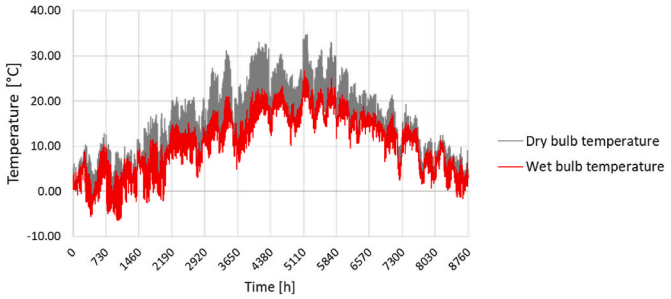

Fig. 13. Dry bulb and wet bulb temperature for a TMY in Ospitaletto.

Table 8
Annual energy flows of ASO substation for the upgrade scenario.

Thermal energy supplied to the user	E_{user}	122.2 MWh
Available waste heat	$E_{WH,ava}$	819.0 MWh
Thermal energy of HP condenser	$E_{co,HP}$	127.9 MWh
Thermal energy of HP evaporator	$E_{ev,HP}$	99.4 MWh
Electrical consumption of HP	$E_{el,HP}$	28.5 MWh
Electrical consumption of pump PM0	$E_{el,PM0}$	0.42 MWh
Electrical consumption of pump PM1	$E_{el,PM1}$	0.66 MWh
Electrical consumption of pump PM2	$E_{el,PM2}$	0.40 MWh
Electrical consumption of pump PM3	$E_{el,PM3}$	2.06 MWh
Total electrical consumption	$E_{el,tot}$	32.0 MWh
Local reuse of waste heat	$E_{WH,local}$	79.2 MWh
Thermal energy drawn from the DH network	$E_{th,consumer}$	20.2 MWh
Thermal energy supplied to the DH network	$E_{th,producer}$	*(*)*

(*) In the upgrade scenario, the substation does not recover heat into the network because the heat demand is not sufficient to accommodate it.

reported in the table. The latter considers not only the pumps for the water circulation within the substation, but also the pumping consumption for the circulation in the distribution circuit of the space heating and domestic how water preparators. The heat supplied by the heat pump condenser is greater than the one supplied to the user because of thermal losses along the circuits and through the thermal storage. The heat extracted by the heat pump evaporator is the sum of the local reuse of waste heat (about 79.5%) and the heat drawn from the thermal network, i.e., from the groundwater wells (about 20.5%). These values show that, while the quantity of available waste heat exceeds the thermal energy needed by the heat pump evaporator, there are times where the substation is anyway forced to extract heat from the district heating network. This happens mainly during Mondays because the factory is in operation, and so there is a heating demand, but the waste heat is not yet available (processes to be cooled and from which the waste heat is recovered start on Tuesday).

As shown in Fig. 14, which refers to a winter period from Monday to Wednesday, the thermal power supplied to the user perfectly matches the demand. This proves correct sizing of the substation components.

The desired supply temperature to the user is ensured by the thermostatic valve TV1, as illustrated in Fig. 15.

When the supply temperature from the storage to the user is higher than the desired setpoint, valve TV1 recirculates a portion of the return flow from the user's facilities to regulate the supply temperature. The brief downward peak, during which the supply temperature falls below the desired setpoint, is related to the initial transient of the heat pump operating cycle. However, this deviation lasts no longer than one timestep, equivalent to 5 min, and the temperature variation remains within 4 °C, thus not significantly impacting user satisfaction. Consequently, the heat pump is able to reliably maintain the required temperature for the user.

A typical winter week, spanning from Monday to Sunday, is represented in Fig. 16.

It shows the thermal power supplied by the heat pump condenser (red line), the thermal power supplied to the user (blue line), and their

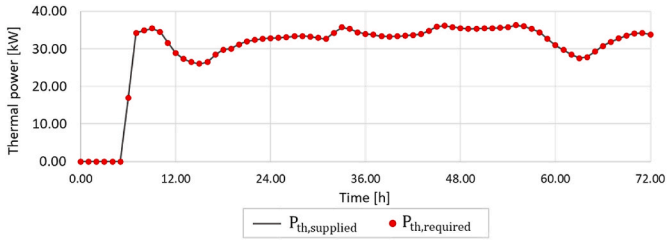

Fig. 14. Thermal power required and supplied to the user from a winter Monday to a winter Wednesday. According to the operating schedule, the thermal power required is zero until 6:00 a.m. of Monday since the factory is closed.

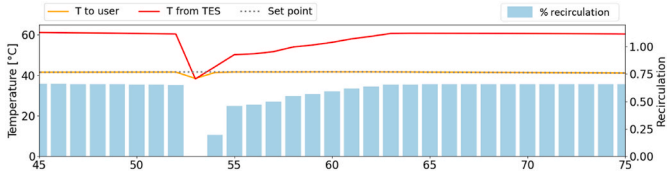

Fig. 15. Operation of thermostatic valve TV1.

difference (grey line) which represents the net thermal power through the storage tank excluding thermal losses. On the right axis, the state of charge of the tank is shown. Thanks to the control logic implemented and described in the methodology section, while the heat is continuously supplied to the user during the operating period of the steel mill, thanks to the storage tank the operation of the heat pump is pulsating. Although the steel mill is closed, during Sunday the state of charge slowly decreases due to thermal losses.

The temperature profile within the storage tank for two charging and discharging cycles is shown in Fig. 17. The water supplied to the user is drawn from the upper part, its temperature is represented by the red line. Temperature detections of the upper and lower sensors, placed at 75 % and 30 % of the tank's height respectively, are indicated by the yellow and light blue lines. The temperature in the bottom part of the storage tank is represented by the blue line. The setpoint temperature of the tank is set to 55 °C (dashed grey line). The activation signal to the heat pump is visualised by the green line.

The thermal stratification in the storage ensures a sufficiently high and approximately constant supply temperature to the user during the period when the heat pump is off. In the simulation, the stratification is almost completely lost during heat pump operation due to high mixing phenomena. The two-sensor control logic is also evident. The heat pump activation signal becomes positive as soon as the temperature detected by the upper sensor is equal to the setpoint. The signal switches off when the setpoint is reached at the height of the lower sensor. Despite the signal being turned off, the storage temperature continues to rise for two timesteps due to the delayed shutdown of the heat pump of about 10 min.

Regarding the COP of the heat pump, Fig. 18 shows the difference between two operating cycles. In the first cycle groundwater wells are

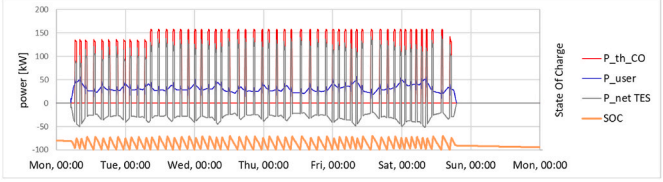

Fig. 16. Thermal powers in substation operation, including user supply, condenser output, and net TES exchange. The right axis shows the TES state of charge (SOC).

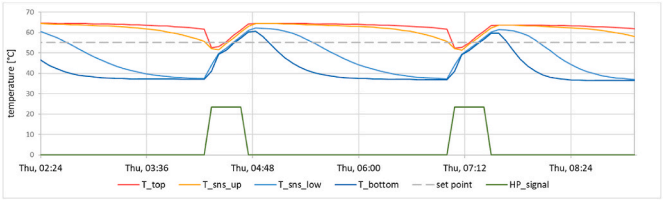

Fig. 17. Temperature profile in the storage tank: readings from four sensors positioned at different heights, along with the heat pump activation signal.

exploited, in the second one the heat pump is fed by the waste heat.

The higher thermal quality of waste heat with respect to groundwater wells allows an increase in heat pump performance. The average COP of the operating cycle increases by about 12%, from 4.1 to 4.6. It should be noted that the second operating cycle refers to a winter period in which waste heat is available at about 25 °C. In summer periods, the higher waste heat temperature allows for an average cycle COP of up to about 5.

In the upper part of Fig. 19 the monthly distribution of the energy flows to the heat pump is shown, including both thermal and electrical inputs. The light red area represents the local reuse of waste heat, the blue area indicates the thermal energy extracted from the groundwater wells through the district heating network, and the light grey area corresponds to the electricity consumed by the heat pump.

In the lower part of Fig. 19, the percentage of thermal energy supplied to the heat pump's evaporator from groundwater wells is shown. The remaining energy is sourced from the waste heat. This distribution remains nearly constant throughout the year, with an average value of approximately 22%.

For each month of the simulated year, the graph in Fig. 20 shows:

- $E_{wh\ available}$: total availability of waste heat according to the size of the heat exchanger and the WH availability profile
- $E_{wh\ local}$: waste heat recovered and used locally by the HP installed at the steel mill
- $E_{wh\ network}$: waste heat recovered and supplied to the district heating network
- $E_{wh\ total}$: total recovered waste heat (sum of local recovery and network recovery)

The local reuse of waste heat is higher during the winter months as heating demand of ASO steel mill is higher. Only about the 9.7% of the total available waste heat is recovered. This means that most of the availability is released into the environment through the cooling towers. The percentage recovered is so low because in the upgrade scenario there is no recovery of waste heat into district heating, indeed total recovery coincides with local recovery. This is because the total heating demand of the entire network is already fully met by the previously installed heat recovery exchanger, which is not part of the analyzed bidirectional substation.

The KPIs of the substation obtained for the upgrade scenario are shown in Table 9.

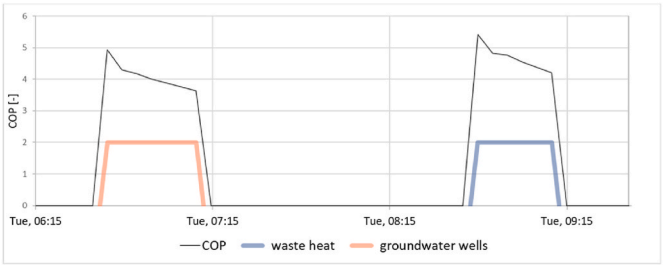

Fig. 18. Dynamic performance of the heat pump.

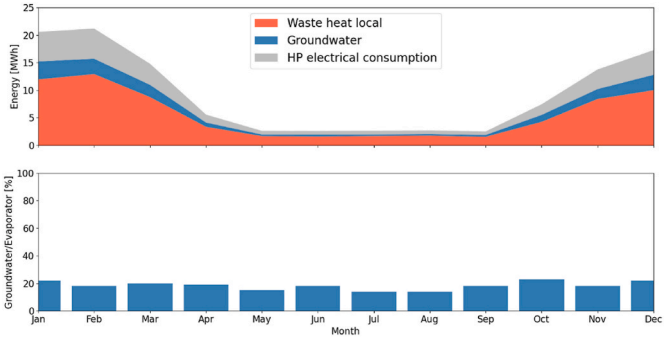

Fig. 19. Monthly distribution of the heat pump's energy inputs.

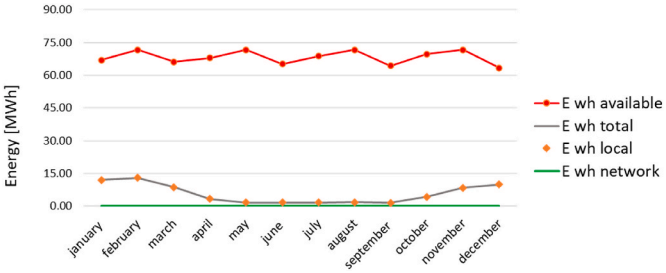

Fig. 20. Waste heat recovery for the upgrade scenario.

The SPF is lower than the SCOP because it accounts for both the thermal losses from the heat storage and distribution pipes, as well as the electricity consumption of all the local circulating pumps. The PEF_{nren} is significantly reduced compared with the typical value of a conventional gas boiler system (about 1.05).

The heat pump operates for approximately 2,400 h annually. Even if there is no waste heat storage system to bridge the temporal mismatch between availability and demand, about 78% of the time the HP is powered by waste heat, operating with an average COP, ranging from 4.3 to 5 based on the WH temperature. While for the remaining period, the HP is sourced by groundwater wells at 15 °C, resulting in an average COP of about 4.1.

4.2. Upgrade vs reference scenario

The results of the comparison between the upgrade and the reference scenario are shown in Table 10.

The replacement of the existing gas boiler system with the low-temperature waste heat recovery substation connected to the district heating network achieves significant benefits. As shown in the table, this change leads to a 73% reduction in non-renewable primary energy consumption and a 75% decrease in greenhouse gas emissions, highlighting the potential for substantial energy and environmental savings.

4.3. Analysis of the optimal upgrade scenario

To evaluate possible future developments of the district heating network in Ospitaletto the analysis of an optimal upgrade scenario is proposed. It is an ideal limit scenario in which it is assumed that all the excess waste heat available for the substation can be recovered in the network because it is required thanks to a network expansion, Fig. 21.

Table 9
KPIs of the waste heat recovery substation at ASO steel mill.

$SCOP_{HP}$	4.49
$SCOP_{HP,TES}$	4.29
SPF	3.82
PEF_{nren}	0.30

Table 10
Non-renewable primary energy and greenhouse gas emissions comparison.

	Reference scenario	Upgrade scenario	Savings
Non-renewable primary energy	134.7 MWh	36.6 MWh	73 %
Greenhouse gas emissions	31.7 $t_{CO2.eq}$	7.84 $t_{CO2.eq}$	75 %

There is a slight difference between the red line and the grey line, barely recognisable in the figure, due to thermal losses. The latter are mainly concentrated in the section of pipework connecting the heat exchanger kit with the heat pump room, about 130 m long.

In this limit scenario the amount of waste heat recovered in the network is equal to 735 MWh, which corresponds to approx. 89.8% of the total availability. To achieve this scenario the addition of new connected users into the district heating system is required. Moreover, it is necessary that they have a heat demand during summer at least equal to the available waste heat. Otherwise, there will still be excess of waste heat released into the environment, unless seasonal thermal storages are planned.

The heat fluxes between the waste heat recovery substation and the district heating network in the optimal upgrade scenario are shown in Fig. 22. The figure presents the fluxes for both a typical winter week, representing the average week of February, and a typical summer week, representing the average week of August. Positive values represent heat extracted from the network by the substation, acting as a consumer, while negative values refer to heat fed back into the network by the substation, acting as a producer.

On Mondays, the absence of waste heat causes the steel mill to act as a consumer. In contrast, for the rest of the week, the available waste heat exceeds the local heating demand, so the steel mill becomes a producer. On Sundays, the substation is disconnected due to the steel mill being closed. During the winter, the heating demand of the steel mill is higher because of space heating, resulting in significantly less waste heat being fed into the network compared to the summer. This heat exchange between the substation and the district heating network is made possible by the bidirectional connection, which allows the heat flow to be reversed according to operating conditions, as illustrated in Fig. 23.

The graph illustrates the thermal power exchanged between the substation and the district heating network (P_{dh}). Positive values correspond to heat extraction from the network (consumer mode), while negative values indicate heat supply to the network (producer mode). The light grey areas highlight periods when the heat pump in the heating module of the ASO substation is operating. Additionally, the graph points out periods when waste heat is available and when it is not. During the period when waste heat is not available, the heat extracted by the heat pump evaporator is drawn from the district heating network. As soon as waste heat becomes available, with a capacity of 150 kW, the substation starts supplying heat to the district heating network. The transition from consumer to producer mode occurs seamlessly due to the hydraulic kit, which regulates system operation based on circulation

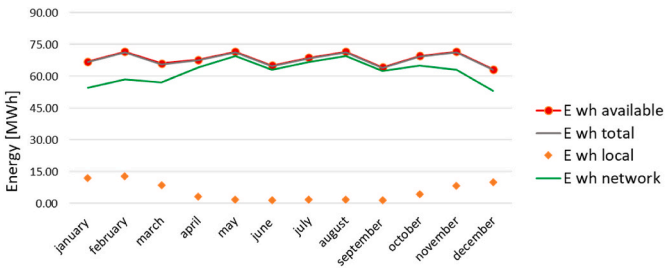

Fig. 21. Waste heat recovery for the optimal upgrade scenario.

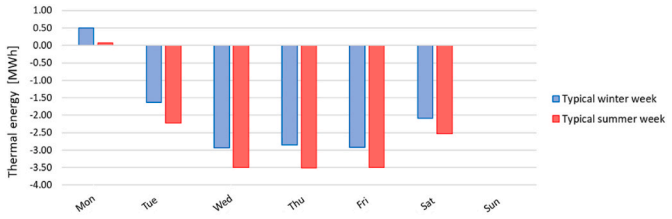

Fig. 22. Heat fluxes between the substation and the DHN for a typical winter and summer week in the optimal upgrade scenario.

pump imbalance. Since the thermal power required by the heat pump evaporator is lower than the capacity of the WH recovery heat exchanger, the substation operates in producer mode even when the heat pump is active, if waste heat is available. These results highlight the significant advantage of the bidirectional connection presented in this study. It enables a rapid inversion of the heat flow and prevents the dissipation of excess available waste heat, even when there is a local heating demand.

The additional electricity consumption for pumping, required to feed the excess waste heat into the network compared to the upgrade scenario, is estimated to be 1.82 MWh. This increase is due to the higher mass flow rate in circulation. The electricity consumption to transport the heat from the steel mill to the connected users is not considered as it concerns the pumps installed in the centralized pumping station of the district heating.

It is worth mentioning that what is recovered is "cold" waste heat, as its thermal level is not suitable to meet users' demands. Therefore, the evaluation of the overall benefits must also consider the electrical consumption of the decentralized heat pumps of the other connected users.

5. Conclusions

This work addresses some of the existing gaps in the integration of low-temperature waste heat recovery into district heating systems, particularly for neutral temperature networks. A bidirectional HP-based substation, capable of adapting its hydraulic configuration to varying operational temperature conditions, is presented and modelled, with its accuracy validated through comparison with measured data from a real case. The novelty lies in the comprehensive design and flexible modelling of a bidirectional substation for thermal prosumers, providing a valuable tool for optimizing waste heat recovery systems across different configurations and operational scenarios in district heating networks.

The model's accuracy has been validated through comparisons with monitoring data taken from a case study, showing that the estimation of the heat pump's COP is fairly accurate, with an error of no more than 3 %. When considering the heat pump and storage unit together, the error in the performance calculation over a period of about 2 months is slightly higher (+4 %), but still within acceptable limits. The Performance Factor of the substation is also accurately estimated, with an error of about 3 %.

In the considered case study, waste heat is recovered from the cooling processes of a foundry and first used to cover the space heating and sanitary hot water needs of the factory, providing the desired temperature levels through a heat pump. Excess waste heat is delivered to a district heating network, which is in turn used to satisfy the aforementioned internal needs in case waste heat is not sufficient.

The case study analysis shows the striking energy efficiency benefits achievable with this approach: compared to a fossil-fuelled heat generator savings of about 75% in both the non-renewable primary energy consumption and greenhouse gas emissions were achieved, assuming the use of grid electricity with the current Italian generation mix. The bidirectional connection of an industry to a district heating network allows maximizing the recovery of its waste heat as any excess with respect to the internal needs can be supplied to other connected users. As observed in the analyzed case study, waste heat is indeed often available in quantities largely exceeding the local heating demand, especially in summer. Specifically, in the studied case, about 90% of the available waste heat was in excess with respect to the industrial site needs of space heating and hot water. This heat can be recovered into the network as far as any demand from other users exists. Finally, the district heating connection also allows covering some of the factory heating needs – e.g., during periods when offices are open, but production is absent or low and not enough waste heat is available. Assuming the district heating system harvests other surrounding sustainable sources (aquifer wells in the case study considered here), this further helps in decarbonizing factory consumptions.

While the model has here been used to analyze a specific demonstration site in Ospitaletto, Italy, it was developed to simulate the operation of a general bidirectional thermal substation and its applicability is hence not limited to the considered example. The model can be applied to different industrial and geographical contexts by appropriately modifying key boundary conditions – such as ambient temperature profile, district heating network temperatures, and connected user load profiles. In fact, type of bidirectional substation described in this work was implemented also in other contexts within the LIFE4HeatRecovery project, with demonstration sites in the Netherlands and Denmark, featuring different temperature levels and waste heat sources [46]. While individual substation configurations slightly varied to meet specific operational needs, the model was designed to be flexible enough to be applicable to these cases as well. It is also worth mentioning that, concerning the technical replicability of these bidirectional substations in practical applications, the main constraint appears not to be given by operational conditions, but rather by the availability of a district heating network in the proximity of the industrial site.

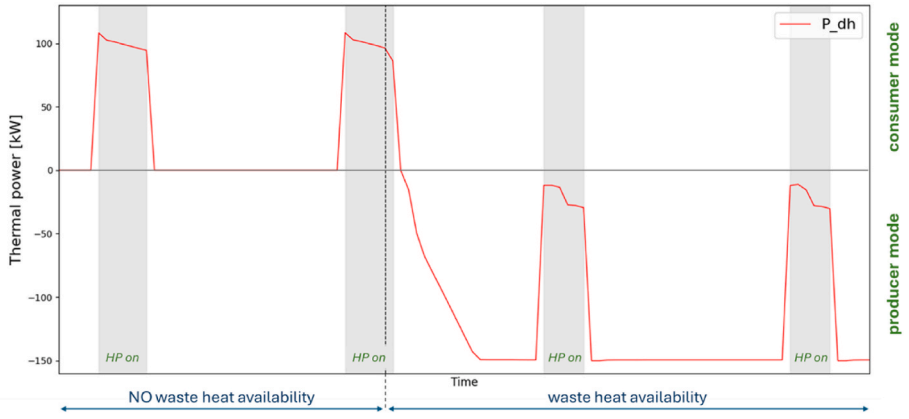

Fig. 23. Heat flux reversal between the DH network and the substation enabled by the bidirectional connection.

Although the proposed model shown good accuracy, some aspects could benefit of further refinement. For instance, the specific prosumer loads are not modelled in detail and are treated as boundary conditions for the substation model. The district heating network is represented by an external temperature profile, which means that the potential impact of the substation operation on network temperatures is not fully assessed. This limitation might be an issue when applying the model to very large industrial sites, with sizes comparable to the local network transmission capacity. Moreover, the model assumes a direct connection between the substation and the network, without a heat exchanger, as in the considered case study. In other situations, an additional heat exchanger at the network interface might exist. To fully account for the corresponding induced temperature difference between the substation circuit and the network, the hydraulic kit model should be slightly modified by adding the heat exchanger component.

An additional development of this work could include economic aspects. While this study focused on the modelling and the energy performance of the proposed substation, a coupling with economic data (investment costs, electricity prices, costs of alternative solutions) would allow to explore the financial feasibility of these applications under different conditions.

This work provides a step forward for the integration of low-temperature waste heat recovery into district heating systems. Though the considered design is tailored to neutral temperature networks, many of the underlying concepts and schemes could be adapted to conventional networks. The offered a flexible and scalable model aims to support the transition toward more sustainable energy systems while addressing critical challenges in waste heat utilization.

CRediT authorship contribution statement

D. Anania: Writing – original draft, Validation, Software, Methodology, Investigation, Data curation, Conceptualization. **G. Russo:** Supervision, Conceptualization. **A. Palombo:** Supervision. **F. Orizio:** Data curation. **R. Fedrizzi:** Supervision. **M. Cozzini:** Supervision, Methodology, Data curation, Conceptualization.

Declaration of competing interest

The authors declare that they have no known competing financial interests or personal relationships that could have appeared to influence the work reported in this paper.

Acknowledgment

The present work is part of the LIFE4HeatRecovery project, funded by the LIFE Programme of the European Union under contract number LIFE17 CCM/IT/000085. The authors would like to warmly thank Francesco Turrin for sharing EURAC's in-house heat pump model, which he implemented in previous research.

Appendix A. Control logic of the substation

Figure A.1 shows the workflow diagram of the control logic for the heating module. The same logic, in a mirrored approach, applies to the cooling module.

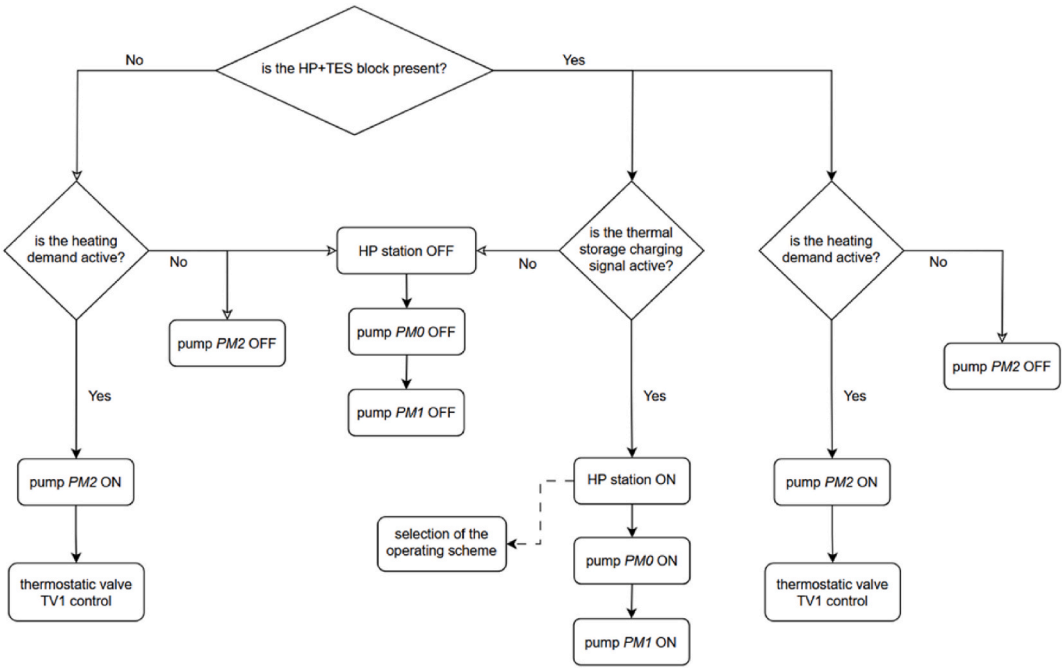

Fig. A.1. Workflow diagram of the control logic of the heating module implemented in the module.

If the HP + TES block is present, the activation of the heat pumps is managed based on the state of charge of the thermal storage, ensuring that the heat pump operates only when needed. This approach allows for flexible management of scenarios where both heating demand and waste heat availability fluctuate, ensuring efficient and adaptive system operation. The selection of the operating scheme is based on the rules provided in [40].

Abbreviations

COP	Coefficient of Performance
DH	District Heating
DHC	District Heating and Cooling
DHN	District Heating Network
DHW	Domestic Hot Water
EU	European Union
HP	Heat Pump
KPI	Key Performance Indicator
LCOH	Levelized Cost of Heat
PEF	Primary Energy Factor
PF	Performance Factor
RMSE	Root Mean Square Error
SCOP	Seasonal Coefficient of Performance
SH	Space Heating
SPF	Seasonal Performance Factor
TES	Thermal Energy Storage
TMY	Typical Meteorological Year
TSP	Temperature Set Point
TV	Thermostatic Valve
WH	Waste Heat

Variables

c_p	specific heat at constant pressure
$\dot{m}$	mass flow rate
A	surface area
D	diameter
E	energy
H	height
H'	pressure head
M	mass
P	power
c	specific heat
f	emission factor
α	convective heat transfer coefficient
η	efficiency
θ	time
λ	thermal conductivity
ρ	density
ω	rotating speed

Subscripts

ava	available
c	compressor
co	condenser
el	electrical
ev	evaporator
ext	external
hex	heat exchanger
ins	insulation
int	internal
med	medium
nren	non-renewable
p	primary
rat	rated
ren	renewable
src	source
th	thermal
wh	waste heat

Data availability

Data will be made available on request.

References

[1] Lund H, Østergaard PA, Connolly D, Mathiesen BV. Smart energy and smart energy systems. Energy 2017;137:556–65. https://doi.org/10.1016/j.energy.2017.05.123.

[2] Heat policy statement: towards decarbonising heat : maximising the opportunities for Scotland. Edinburgh: Scottish Government; 2015.

[3] Revesz A, Jones P, Dunham C, Davies G, Marques C, Matabuena R, Scott J, Maidment G. Developing novel 5th generation district energy networks. Energy 2020;201:117389. https://doi.org/10.1016/j.energy.2020.117389.

[4] European Environment Agency. Greenhouse gas emissions from energy use in buildings in Europe, (n.d.). https://www.eea.europa.eu/data-and-maps/indicators/greenhouse-gas-emissions-from-energy/assessment.

[5] District Heating – Analysis, IEA (n.d.). https://www.iea.org/reports/district-heating.

[6] Papapetrou M, Kosmadakis G, Cipollina A, La Commare U, Micale G. Industrial waste heat: estimation of the technically available resource in the EU per industrial sector, temperature level and country. Appl Therm Eng 2018;138:207–16. https://doi.org/10.1016/j.applthermaleng.2018.04.043.

[7] Jouhara H, Khordehgah N, Almahmoud S, Delpech B, Chauhan A, Tassou SA. Waste heat recovery technologies and applications. Therm Sci Eng Prog 2018;6:268–89. https://doi.org/10.1016/j.tsep.2018.04.017.

[8] Xu ZY, Wang RZ, Yang C. Perspectives for low-temperature waste heat recovery. Energy 2019;176:1037–43. https://doi.org/10.1016/j.energy.2019.04.001.

[9] Lund H, Werner S, Wiltshire R, Svendsen S, Thorsen JE, Hvelplund F, Mathiesen BV. 4th generation district heating (4GDH). Energy 2014;68:1–11. https://doi.org/10.1016/j.energy.2014.02.089.

[10] Buonomano A, Forzano C, Mongibello L, Palombo A, Russo G. Optimising low-temperature district heating networks: a simulation-based approach with experimental verification. Energy 2024;304:131954. https://doi.org/10.1016/j.energy.2024.131954.

[11] Giuzio GF, Russo G, Forzano C, Del Papa G, Buonomano A. Evaluating the cost of energy flexibility strategies to design sustainable building clusters: Modelling and multi-domain analysis. Energy Rep 2024;12:656–72. https://doi.org/10.1016/j.egyr.2024.06.047.

[12] Fang H, Xia J, Jiang Y. Key issues and solutions in a district heating system using low-grade industrial waste heat. Energy 2015;86:589–602. https://doi.org/10.1016/j.energy.2015.04.052.

[13] Wahlroos M, Pärssinen M, Manner J, Syri S. Utilizing data center waste heat in district heating – impacts on energy efficiency and prospects for low-temperature district heating networks. Energy 2017;140:1228–38. https://doi.org/10.1016/j.energy.2017.08.078.

[14] Khosravi A, Laukkanen T, Vuorinen V, Syri S. Waste heat recovery from a data centre and 5G smart Poles for low-temperature district heating network. Energy 2021;218:119468. https://doi.org/10.1016/j.energy.2020.119468.

[15] Fitó J, Hodencq S, Ramousse J, Wurtz F, Stutz B, Debray F, Vincent B. Energy- and exergy-based optimal designs of a low-temperature industrial waste heat recovery system in district heating. Energy Convers Manag 2020;211:112753. https://doi.org/10.1016/j.enconman.2020.112753.

[16] Fang H, Xia J, Zhu K, Su Y, Jiang Y. Industrial waste heat utilization for low temperature district heating. Energy Policy 2013;62:236–46. https://doi.org/10.1016/j.enpol.2013.06.104.

[17] Li Y, Xia J, Fang H, Su Y, Jiang Y. Case study on industrial surplus heat of steel plants for district heating in northern China. Energy 2016;102:397–405. https://doi.org/10.1016/j.energy.2016.02.105.

[18] Lund R, Persson U. Mapping of potential heat sources for heat pumps for district heating in Denmark. Energy 2016;110:129–38. https://doi.org/10.1016/j.energy.2015.12.127.

[19] Brange L, Englund J, Lauenburg P. Prosumers in district heating networks – a Swedish case study. Appl Energy 2016;164:492–500. https://doi.org/10.1016/j.apenergy.2015.12.020.

[20] Brand L, Calvén A, Englund J, Landersjö H, Lauenburg P. Smart district heating networks – a simulation study of prosumers' impact on technical parameters in distribution networks. Appl Energy 2014;129:39–48. https://doi.org/10.1016/j.apenergy.2014.04.079.

[21] Huang P, Copertaro B, Zhang X, Shen J, Löfgren I, Rönnelid M, Fahlen J, Andersson D, Svanfeldt M. A review of data centers as prosumers in district energy systems: renewable energy integration and waste heat reuse for district heating. Appl Energy 2020;258:114109. https://doi.org/10.1016/j.apenergy.2019.114109.

[22] Postnikov I, Stennikov V, Penkovskii A. Prosumer in the district heating systems: operating and reliability modeling. Energy Proc 2019;158:2530–5. https://doi.org/10.1016/j.egypro.2019.01.411.

[23] Kauko H, Kvalsvik KH, Rohde D, Nord N, Utne Å. Dynamic modeling of local district heating grids with prosumers: a case study for Norway. Energy 2018;151:261–71. https://doi.org/10.1016/j.energy.2018.03.033.

[24] Nord N, Shakerin M, Tereshchenko T, Verda V, Borchiellini R. Data informed physical models for district heating grids with distributed heat sources to understand thermal and hydraulic aspects. Energy 2021;222:119965. https://doi.org/10.1016/j.energy.2021.119965.

[25] Li H, Hou J, Hong T, Nord N. Distinguish between the economic optimal and lowest distribution temperatures for heat-prosumer-based district heating systems with short-term thermal energy storage. Energy 2022;248:123601. https://doi.org/10.1016/j.energy.2022.123601.

[26] Pipiciello M, Trentin F, Soppelsa A, Menegon D, Fedrizzi R, Ricci M, Di Pietra B, Sdringola P. The bidirectional substation for district heating users: experimental performance assessment with operational profiles of prosumer loads and distributed generation. Energy Build 2024;305:113872. https://doi.org/10.1016/j.enbuild.2023.113872.

[27] Lickleder T, Hamacher T, Kramer M, Perić VS. Thermohydraulic model of smart thermal grids with bidirectional power flow between prosumers. Energy 2021;230:120825. https://doi.org/10.1016/j.energy.2021.120825.

[28] Gummerus P. New developments in substations for district heating. In: Advanced district heating and cooling (DHC) systems. Elsevier; 2016. p. 215–21. https://doi.org/10.1016/B978-1-78242-374-4.00010-0.

[29] Wirtz M, Kivilip L, Remmen P, Müller D. Quantifying demand balancing in bidirectional low temperature networks. Energy Build 2020;224:110245. https://doi.org/10.1016/j.enbuild.2020.110245.

[30] Wirtz M, Neumaier L, Remmen P, Müller D. Temperature control in 5th generation district heating and cooling networks: an MILP-based operation optimization. Appl Energy 2021;288:116608. https://doi.org/10.1016/j.apenergy.2021.116608.

[31] Tang H, Liu Y, Chen Y, Wang D, Yuan X. Distributed solar heating system with busbar thermal reservoir network: dynamic modeling and techno-economic analysis. Appl Therm Eng 2024;246:122987. https://doi.org/10.1016/j.applthermaleng.2024.122987.

[32] Lickleder T, Zinsmeister D, Lukas L, Speer F, Hamacher T, Perić VS. Control of bidirectional prosumer substations in smart thermal grids: a weighted proportional-integral control approach. Appl Energy 2024;354:122239. https://doi.org/10.1016/j.apenergy.2023.122239.

[33] Abugabbara M, Lindhe J, Javed S, Bagge H, Johansson D. Modelica-based simulations of decentralised substations to support decarbonisation of district heating and cooling. Energy Rep 2021;7:465–72. https://doi.org/10.1016/j.egyr.2021.08.081.

[34] Abugabbara M, Javed S, Johansson D. A simulation model for the design and analysis of district systems with simultaneous heating and cooling demands. Energy 2022;261:125245. https://doi.org/10.1016/j.energy.2022.125245.

[35] Sdringola P, Ricci M, Ancona MA, Gianaroli F, Capodaglio C, Melino F. Modelling a prototype of bidirectional substation for district heating with thermal prosumers. Sustainability 2023;15:4938. https://doi.org/10.3390/su15064938.

[36] Dino GE, Catrini P, Buscemi A, Piacentino A, Palomba V, Frazzica A. Modeling of a bidirectional substation in a district heating network: validation, dynamic analysis, and application to a solar prosumer. Energy 2023;284:128621. https://doi.org/10.1016/j.energy.2023.128621.

[37] Calixto S, Cozzini M, Manzolini G. Modelling of an existing neutral temperature district heating network: detailed and approximate approaches. Energies 2021;14:379. https://doi.org/10.3390/en14020379.

[38] Calixto S, Köseoğlu C, Cozzini M, Manzolini G. Monitoring and aggregate modelling of an existing neutral temperature district heating network. Energy Rep 2021;7:140–9. https://doi.org/10.1016/j.egyr.2021.08.162.

[39] Verhoeven R, Eijdems H, Wenmeckers M, Harcouët-Menou V. Update (Geo-) Thermal Smart Grid Mijnwater Heerlen 2016. Strasbourg, France.

[40] Andrés M, Thorsen JE, Buffa S, Firan ML, Regidor M, Fedrizzi R. Packaged substations configurations, REWARDHeat. 2021.

[41] Multiport store model for TRNSYS, (n.d.). https://www.trnsys.de/static/788c19e80e1b4e690b35e44b05c8b164/ts_type_340_de.pdf.

[42] PVGIS Online Tool - EU Science Hub, (n.d.). https://re.jrc.ec.europa.eu/pvg_tools/en/.

[43] ISPRA, Indicatori di efficienza e decarbonizzazione del sistema energetico nazionale e del settore elettrico, n.d.

[44] M. Thrower, Series 15 ¦ Module 02 ¦ Boilers & Burners, (n.d.).

[45] Casasso A, Capodaglio P, Simonetto F, Sethi R. Environmental and economic benefits from the phase-out of residential oil heating: a study from the aosta valley region (Italy). Sustainability 2019;11:3633. https://doi.org/10.3390/su11133633.

[46] D. Anania, M. Cozzini, Educational kit – Action E.2, (n.d.). https://www.life4heatrecovery.eu/gallery/E2_20240909_Educational_Kit.pdf (accessed March 15, 2025).